Molecular Therapy
Oncology
Original Article

Targeting the ribosome to treat multiple myeloma

Kylee H. Maclachlan,[1,2,3,9,11] Kezia Gitareja,[4,5,11] Jian Kang,[4,5] Andrew Cuddihy,[1,10] Yuxi Cao,[1,2,3] Nadine Hein,[6] Carleen Cullinane,[1] Ching-Seng Ang,[7] Natalie Brajanovski,[1] Richard B. Pearson,[1,2,8] Amit Khot,[2,3] Elaine Sanij,[1,2,4,5,8,12] Ross D. Hannan,[6,8,12] Gretchen Poortinga,[1,2,12] and Simon J. Harrison[1,2,3,12]

[1]Cancer Research Division, Peter MacCallum Cancer Centre, Melbourne, VIC, Australia; [2]Sir Peter MacCallum Department of Oncology, University of Melbourne, Melbourne, VIC, Australia; [3]Clinical Hematology, Peter MacCallum Cancer Centre, Melbourne, VIC, Australia; [4]St Vincent's Institute of Medical Research, Melbourne, VIC, Australia; [5]Department of Medicine- St Vincent's Hospital, University of Melbourne, Melbourne, VIC, Australia; [6]The ACRF Department of Cancer Biology and Therapeutics, The John Curtin School of Medical Research, Australian National University, Canberra, ACT, Australia; [7]The Bio21 Institute of Molecular Science and Biotechnology Institute, University of Melbourne, Melbourne, VIC, Australia; [8]Department of Biochemistry and Molecular Biology, Monash University, Melbourne, VIC, Australia

The high rates of protein synthesis and processing render multiple myeloma (MM) cells vulnerable to perturbations in protein homeostasis. The induction of proteotoxic stress by targeting protein degradation with proteasome inhibitors (PIs) has revolutionized the treatment of MM. However, resistance to PIs is inevitable and represents an ongoing clinical challenge. Our first-in-human study of the selective inhibitor of RNA polymerase I transcription of ribosomal RNA genes, CX-5461, has demonstrated a potential signal for anti-tumor activity in three of six heavily pre-treated MM patients. Here, we show that CX-5461 has potent anti-myeloma activity in PI-resistant MM preclinical models *in vitro* and *in vivo*. In addition to inhibiting ribosome biogenesis, CX-5461 causes topoisomerase II trapping and replication-dependent DNA damage, leading to G2/M cell-cycle arrest and apoptotic cell death. Combining CX-5461 with PI does not further enhance the anti-myeloma activity of CX-5461 *in vivo*. In contrast, CX-5461 shows synergistic interaction with the histone deacetylase inhibitor panobinostat in both the Vk*MYC and the 5T33-KaLwRij mouse models of MM by targeting ribosome biogenesis and protein synthesis through distinct mechanisms. Our findings thus provide strong evidence to facilitate the clinical development of targeting the ribosome to treat relapsed and refractory MM.

INTRODUCTION

Multiple myeloma (MM) is a clonal plasma cell malignancy that is characterized by proliferation of malignant plasma cells in the bone marrow and the production of large quantities of monoclonal immunoglobins.[1,2] The exceptionally high rates of protein synthesis and processing render MM cells vulnerable to perturbations in protein homeostasis such as inhibition of protein degradation, which normally occurs through polyubiquitination and transporting of proteins to the proteasome. Targeting protein degradation by proteasome inhibitors (PIs) results in the accumulation of misfolded or unfolded proteins in the endoplasmic reticulum (ER) leading to ER stress, which subsequently impedes cell-cycle progression and activates apoptotic pathways leading to cell death.[3] PIs are a cornerstone treatment for MM patients both in frontline and relapsed and refractory MM (RRMM) settings.[4] However, resistance to this treatment modality is inevitable and represents a clinical challenge. Multiple mechanisms have been reported to mediate resistance to PIs, including aberrant expression of proteasomal subunits, heat shock protein induction, and restoring ER homeostasis.[3,5,6] Despite extensive research, these mechanisms are not yet widely validated in patients' samples of RRMM and thus their clinical relevance remains uncertain. In a recent study, gene expression signatures of ribosome and polysome and translation initiation were found to be associated with suboptimal response to the PI bortezomib in MM patient samples,[7] implicating deregulation of ribosome function and altered mRNA translation activity in mediating resistance to PI.

The production of ribosomes involves the synthesis and processing of ribosomal RNAs (rRNAs), assembly of rRNAs and ribosomal proteins in the nucleoli, and transport of pre-ribosomal subunits to the cytoplasm to form functional ribosomes for mRNA translation.[8] The rates of ribosome biogenesis and mRNA translation are controlled by key oncogenic pathways, particularly phosphatidylinositol 3-kinase (PI3K)/protein kinase B (AKT)/ mammalian target of rapamycin complex 1 (mTORC1), RAS/mitogen-activated protein kinase (MAPK) pathways and MYC.[9–11] The first-in-class selective inhibitor of ribosome biogenesis, CX-5461 (Pidnarulex), targets RNA polymerase I (Pol I) transcription of the 47S rRNA genes, a rate-limiting step in ribosome biogenesis. We and other groups have reported the anti-tumor activity of CX-5461 in multiple preclinical models of blood and solid cancers.[12–22] We recently reported the

Received 30 November 2023; accepted 2 February 2024;
https://doi.org/10.1016/j.omton.2024.200771.

[9]Present address: Myeloma Service, Memorial Sloan Kettering Cancer Center, New York, USA

[10]Present address: Paul Albrechtsen Research Institute at CancerCare Manitoba, Winnipeg, Manitoba, Canada

[11]These authors contributed equally

[12]Senior author

Correspondence: Elaine Sanij, St Vincent's Institute of Medical Research, Melbourne, VIC, Australia.
E-mail: esanij@svi.edu.au

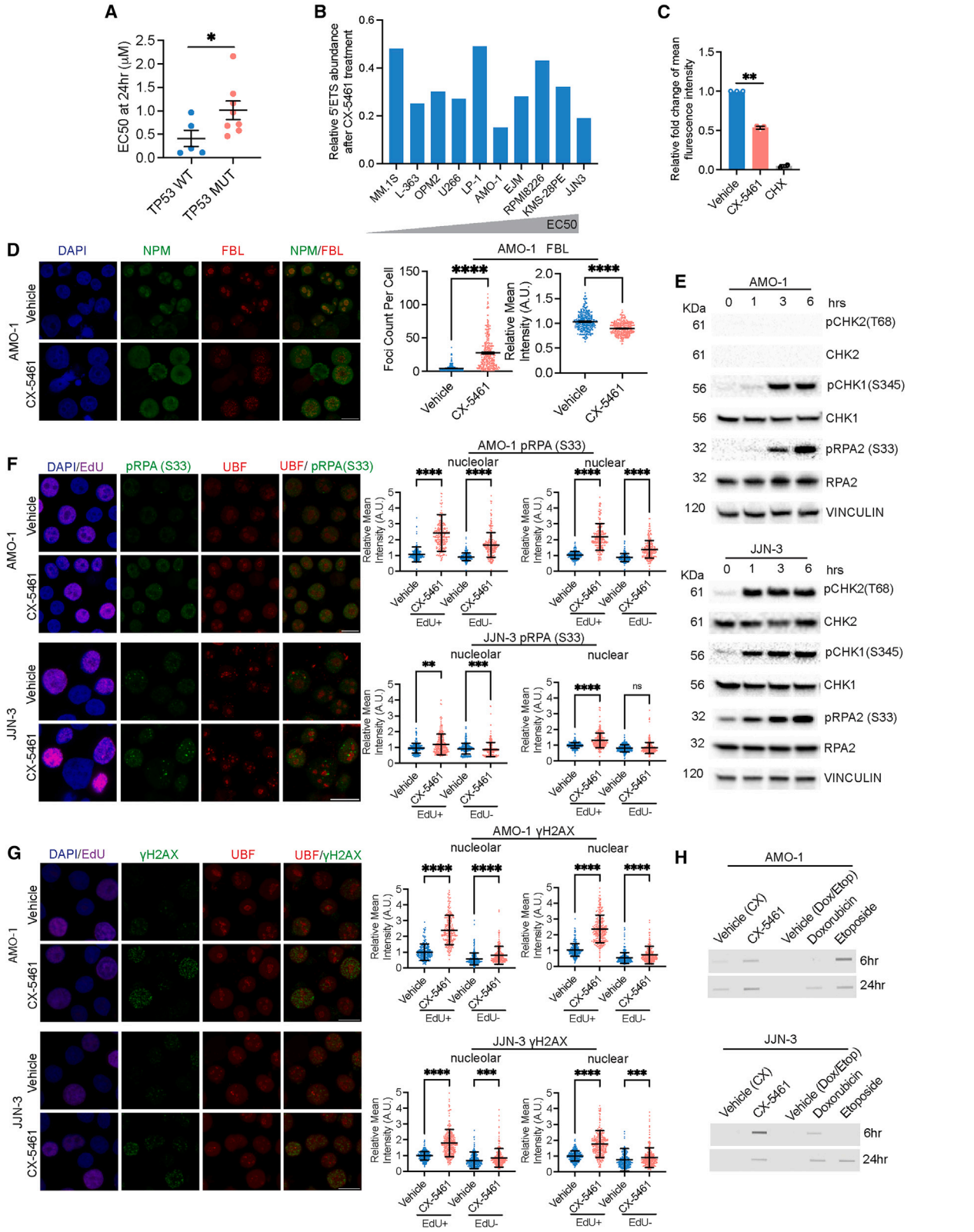

(legend on next page)

results of the first-in-human phase I clinical study of CX-5461 as a single agent in 17 heavily pre-treated patients with refractory blood cancers.[23] In this study, the best response of stable disease was noted in patients with RRMM: three out of six RRMM patients, with actively progressing disease at study entry, maintained disease stabilization for 4–6 cycles. Adding to our understanding of this compound's mechanism, CX-5461 also recently demonstrated clinically significant and durable benefits in patients with homologous recombination (HR)-deficient tumors.[24] This is due to its newly recognized mode of action in acting as a topoisomerase II (TOP2) poison with high selectivity to genomic regions of high transcriptional activity and enrichments with G-quadruplex (G4) DNA structures.[20,25,26] CX-5461 can thus induce replication stress, which, in the absence of a functional HR pathway, leads to DNA damage and cancer cell death.[18] The US Food and Drug Administration (FDA) has recently granted a fast-track designation to CX-5461 for patients with HR-deficient ovarian and breast cancers.

In this paper, we demonstrate that the dual modes of action of CX-5461 in inhibiting ribosome biogenesis and activating replication-dependent DNA damage response (DDR) signaling contribute to its potent anti-myeloma activity in human MM cells and PI-resistant murine MM cells. Here, we have examined strategies of drug combinations with the standard-of-care therapies in MM. We have identified that CX-5461 and the histone deacetylase inhibitor panobinostat exhibit significant synergistic interactions against MM both *in vitro* and *in vivo*. This improved therapeutic benefit is mediated via divergent pathways that enhance the suppression of mRNA translation and protein synthesis in MM cells.

RESULTS

CX-5461 impairs ribosome biogenesis and activates DDR signaling in MM cells

To characterize the molecular actions of CX-5461 in MM, we tested its efficacy across a panel of human MM cell lines (HMCLs), containing a range of cytogenetic translocations and molecular drivers known to be critical in the pathogenesis and prognosis in MM (Table S1). These cell lines demonstrate a wide range of sensitivity to CX-5461 (Figure S1A). As observed previously in lymphoma and acute myeloid leukemia (AML) cells,[14,15] sensitivity of HMCLs to CX-5461 correlates with *TP53* mutation status, with p53 wild-type (WT) cell lines showing significantly lower half-maximal effective concentration (EC50) values (the concentration that induces 50% cell death) than p53 mutant cell lines (Figure 1A). CX-5461 caused apoptotic cell death in p53 WT and mutant HMCLs (Figure S1B) and a G2/M cell-cycle arrest in both p53 WT and p53 null HMCLs (Figure S1C).

CX-5461 selectively inhibits Pol I transcription relative to Pol II and Pol III transcription by inhibiting Pol I recruitment to the rRNA gene promoters.[14,15,18,27–30] In accordance with previous work, inhibition of Pol I transcription by CX-5461 reduced the expression of the 47S rRNA precursor within 1 h in all HMCLs tested (Figure 1B). A decrease in protein synthesis rates, measured by incorporation of methionine analogue L-azidohomoalanine (AHA), was also observed (Figure 1C).

Disruptions in Pol I transcription and ribosome biogenesis lead to nucleolar stress.[31] As expected, prominent changes in nucleolar morphology, indicative of nucleolar stress, were observed within 3 h of CX-5461 treatment as indicated by fragmentation and reduced intensity of the nucleolar protein fibrillarin (FBL) and altered distribution of nucleophosmin (NPM) (Figures 1D and S1D). In addition to inhibiting Pol I transcription initiation, CX-5461 can also induce alterations in rRNA gene chromatin structure and provoke replication stress that activates ataxia telangiectasia mutated (ATM)/ATR signaling within the nucleoli.[18,32,33] Increased phosphorylation of checkpoint kinase 1 (CHK1) at S345 was observed in p53 WT AMO-1 cells, while activation of checkpoint kinase 2 (pCHK2 at T68) was absent due to the lack of CHK2 (Figure 1E). An increase in S33 phosphorylation of the single-strand DNA (ssDNA)-binding protein replication protein A2 (RPA2) was also detected upon

Figure 1. CX-5461 impairs ribosome biogenesis and induces the DDR in MM cells

(A) CX-5461 EC50 doses that induce 50% cell death at 24 h in HMCLs. Cell death was measured by the propidium iodide exclusion assay and the values of EC50 are outlined in Figure S1A. Error bars represent mean ± SEM. Statistical analysis was performed using two-tailed one-way ANOVA Mann-Whitney test. *$p < 0.05$. (B) CX-5461 reduces Pol I transcription rates in MM cells. Cells were treated with 1 μM CX-5461 for 1 h and the abundance of 47S pre-rRNA 5′ETS transcript was measured by quantitative real-time PCR and normalized to β-2-microglobulin and expressed as fold change relative to corresponding vehicle control. Primer sequenced are listed in Table S5. The cell lines are ordered based on EC50 values of CX-5461 doses from low to high values. (C) AMO-1 cells were treated with either vehicle, 0.5 μM CX-5461, or cycloheximide (CHX) 100 μg/mL (a control for inhibiting protein synthesis) for 6 h, and labeled with 50 μM L-azidohomoalanine for 1 h before fixing. The newly synthesized proteins were labeled with Alexa Fluor 488-azide by Click chemistry and analyzed by flow cytometry. Error bars represent mean ± SEM (n = 3). Statistical analysis was performed using one sample t test. **$p < 0.01$. (D) Co-IF assays of fibrillarin (FBL) and nucleophosmin (NPM) in AMO-1cells treated with 0.5 μM CX-5461 or vehicle for 3 h. Representative images of two biologically independent experiments. Scale bar, 10 μm. Signal intensities were analyzed using CellProfiler. Raw mean intensity values were normalized to the median value of the vehicle control. Error bars represent mean ± SD. Statistical analysis was performed using a two-tailed nonparametric Mann-Whitney t test. ****$p < 0.0001$. (E) Western blotting of cells treated with 0.5 μM CX-5461. Vinculin was probed as a loading control. Representative images of n = 3. (F) Co-IF analysis of pRPA S33 and the nucleolar protein UBF in cells treated with 0.5 μM CX-5461 or vehicle for 3 h. Cells were pulse labeled with EdU 30 min prior to drug treatment. (G) Co-IF analysis of γH2AX with UBF in cells treated as (F). (F and G) Scale bar, 10 μm. Quantification of nucleolar (signal overlap with UBF) and nuclear (signal overlap with DAPI) of pRPA S33 (F) or γH2AX (G) signal intensity was performed using CellProfiler. n = 300 EdU+ and n = 300 EdU-negative cells per treatment condition were analyzed over three or four biologically independent experiments. Raw mean intensity values were normalized to the median value of vehicle control. Error bars represent mean ± SD. Statistical analysis was performed using one-way ANOVA, Kruskal-Wallis multiple comparisons test. ****$p < 0.0001$, ***$p < 0.001$, **$p < 0.01$; ns, non-significant with $p > 0.05$. (H) RADAR assay. DNA-protein covalent complexes were isolated and TOP2α probed. Representative images of n = 3.

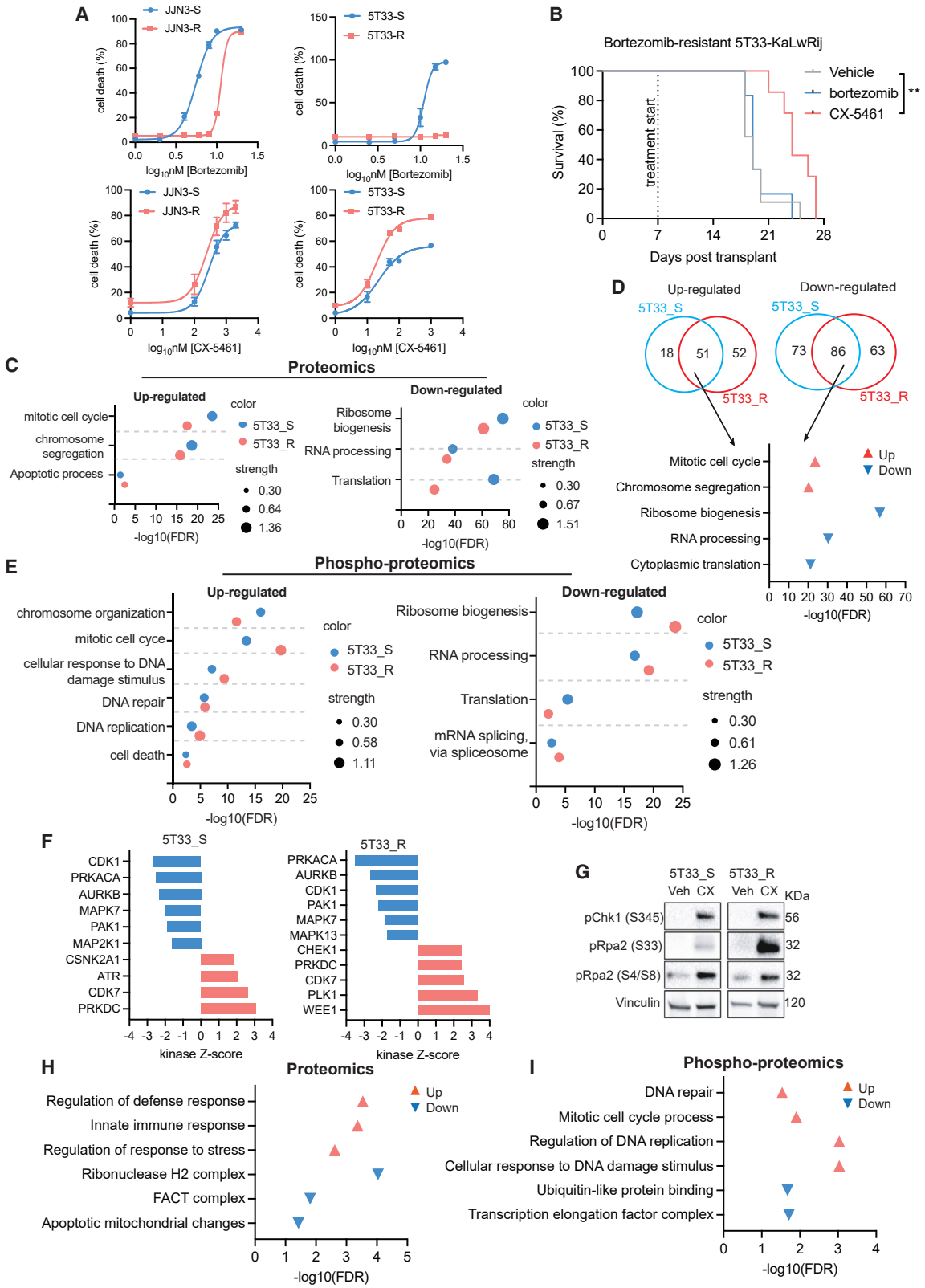

(legend on next page)

CX-5461 treatment, indicating replication stress. Consistently, increased pCHK1 S345, pCHK2 T68, and pRPA2 S33 were also observed in p53 null JJN-3 cells within 1 h of exposure. Thus, our data corroborate previous findings that CX-5461 induces replication stress and activates DDR. We next assessed CX-5461-mediated replication stress by co-immunofluorescence (co-IF) staining of pRPA2 S33 with the Pol I transcription factor upstream binding factor (UBF). Induction of pRPA2 S33, indicating the presence of ssDNA lesions, was observed within nucleoli and across the nucleus in both EdU-positive (S-phase) and EdU-negative cell populations following treatment with CX-5461 (Figures 1F and S1E). Co-IF analysis of the DNA double-strand breaks (DSBs) marker γH2A.X (phosphorylated histone H2A.X on serine 139) and UBTF also demonstrated the induction of γH2A.X foci within the nucleoli and throughout the nucleus (Figures 1G and S1F). Notably, γH2A.X foci are mainly induced in EdU-positive cell populations, suggesting that CX-5461-induced DNA damage is dependent on DNA replication.

CX-5461 has been reported to act as a TOP2 inhibitor[25] and is proposed to act as a DNA-structure-driven TOP2 poison via selective targeting of transcriptionally active regions bearing G4 DNA or R-loops structures, which are enriched at the rRNA genes. This, in turn, leads to an increase in topological stress that recruits and facilitates TOP2a trapping.[34] TOP2a alleviates topological stress during transcription or replication by forming a transient TOP2a-DNA covalent complex (TOP2cc) and producing temporary DSBs. TOP2 inhibitors stabilize transient TOP2cc, leading to accumulation of cytotoxic DSBs, which may contribute to CX-5461-mediated DDR. We thus assessed CX-5461's TOP2a trapping activity by performing rapid approach to DNA-adduct recovery (RADAR) assays (Figures 1H and S1G). We observed that, similar to TOP2 poisons doxorubicin and etoposide, CX-5461 also trapped TOP2a onto the DNA. Collectively, our data demonstrate that CX-5461 induces replication-dependent DNA damage through stabilizing TOP2cc at the rRNA genes and across the genome, leading to replication stress, activation of cell-cycle checkpoints, and eventually cell death.

CX-5461 has potent activity in PI-resistant MM models

Restoration of protein homeostasis has been suggested to contribute to resistance to PIs in MM.[7] We therefore propose that targeting the ribosome is an effective approach to treat PI-resistant MM. To test this hypothesis, we generated bortezomib-resistant p53 null JJN3 HMCL (referred to as JJN3_R) and 5T33 mouse MM cell line (referred to as 5T33_R) by culturing cells in increasing concentrations of bortezomib over 6 months. The parental cell lines were cultured concurrently without drug treatment (referred to as JJN3_S and 5T33_S cells). Resistance to bortezomib was confirmed by measuring cell death following treatment (Figure 2A). Strikingly, PI-resistant cells exhibited higher sensitivity to CX-5461 than parental counterparts (Figure 2A). We subsequently transplanted 5T33_R cells into C57BL6/KaLwRij mice, which is considered an aggressive immunocompetent model involving multiple genetic events (including loss of *FGFR3*, *RB1*, *CARD11* and gain of *AKT1*, *CCND1*)[35,36] and not only confirmed bortezomib resistance *in vivo* but also observed that CX-5461 provides a significant survival benefit against PI-resistant MM (Figure 2B).

To characterize the molecular response to CX-5461 in the context of PI resistance, we performed label-free quantitative proteomic analysis in both parental and PI-resistant 5T33 cells following CX-5461 treatment for 24 h (Figures S2A and S2B). We identified 253 and 228 were differentially expressed in 5T33_S cells and 5T33_R cells upon CX-5461 treatment, respectively (Table S3). Gene Ontology enrichment analysis showed similar biological processes that were altered by CX-5461 in parental and PI-resistant cells (Figure 2C). Within the top-ranked processes in both cell lines, we observed increased expression of proteins belonging to mitotic cell-cycle, chromosome segregation, and apoptotic process processes and decreased expression of factors involved in ribosome biogenesis, RNA processing, and translation. Furthermore, more than 50% of the differentially expressed proteins were shared by both parental and PI-resistant cells and enriched in the processes involved in cell cycle, ribosome biogenesis, and mRNA translation (Figure 2D). These results thereby demonstrate the potency of CX-5461 in inhibiting cell-cycle progression, ribosome biogenesis, and mRNA translation in PI-resistant cellular context.

To further determine the signaling pathways regulated by CX-5461, we performed label-free phosphoproteomic analysis. We identified 4253 phospho-sites of which 379 and 325 phospho-sites were differentially regulated in parental and 5T33_R cells upon CX-5461 treatment, respectively (Figures S2C and S2D; Table S4). Gene Ontology

Figure 2. CX-5461 has potent activity in PI-resistant MM models

(A) Culture-adapted bortezomib-resistant human JJN-3 and murine 5T33 myeloma cells and parental controls were treated with bortezomib (upper) and CX-5461 (bottom) for 72 h and cell death was measured using propidium iodide exclusion assay. Error bars represent mean ± SEM of n = 3. (B) C57BL-KaLwRij mice were transplanted with bortezomib-resistant 5T33 cells and treated with either 5 mg/kg bortezomib via i.p. injection weekly, 35 mg/kg CX-5461 via oral gavage twice weekly, or the vehicle control (n = 6 per group). Kaplan-Meier plot is shown. Statistical analysis was performed using log rank test. $^{**}p < 0.01$. (C) Label-free quantitative proteomic analyses of parental and bortezomib-resistant 5T33 cells treated with 0.5 μM CX-5461 or vehicle for 24 h. Gene Ontology enrichment analysis identified the top-ranked biological processes regulated by CX-5461. (D) Gene Ontology enrichment analyses of differentially expressed proteins shared by both 5T33_S and 5T33_R cells identified the top-ranked biological processes regulated by CX-5461. (E) Quantitative phosphoproteomic analyses of parental and bortezomib-resistant 5T33 cells treated with 0.5 μM CX-5461 or vehicle for 24 h. Gene Ontology enrichment analysis identified the top-ranked biological processes regulated by CX-5461. (F) The most significantly upregulated and downregulated kinases ($p < 0.05$, substrates ≥ 3) identified from kinase-substrate enrichment analysis using Phosphomatics (version 2.0) are shown and ranked by the kinase *Z* scores. (G) Cells were treated with 0.5 μM CX-5461 or vehicle for 24 h and protein lysates collected for western blotting. Vinculin was probed as a loading control. Representative images of n = 3. (H and I) Gene Ontology enrichment analyses of differentially expressed proteins (H) and differently phosphorylated proteins (I) in bortezomib-resistant cells relative to parental cells identified the top-ranked biological processes associated with bortezomib resistance.

analysis identified an enrichment in the biological processes related to mitosis and DNA replication in CX-5461-treated cells (Figure 2E). Notably, signatures related to cellular response to DNA damage stimulus and DNA repair were also identified upon CX-5461 treatment (Figure 2E). The upstream kinase activity inferred from the substrate phosphorylation data using KEA3[37] and Phosphomatics[38] identified ATR-CHEK1 and ATM-CHEK2 signaling activities to be significantly upregulated in both parental and PI-resistant 5T33_R cells treated with CX-5461 (Figures 2F and S2E), strongly supporting that CX-5461 induces DDR signaling in MM cells (Figure 2G).

To explore the mechanisms associated with bortezomib resistance in 5T33_R cells, we analyzed proteomic and phosphoproteomic data by comparing untreated 5T33_R cells to parental 5T33_S cells. Increased expression of Psmb5 and downregulation of apoptotic mitochondrial changes were found in resistant cells, which may reduce on-target effects of bortezomib and enhance cell survival (Figure 2H; Table S3). Our data, surprisingly, showed regulation of defense response and innate immune response to be the top-ranked biological processes of genes associated with antigen processing and presentation and cytokine production being significantly upregulated in resistant cells, suggesting increased immunogenicity (Figures 2H and S2F). This is consistent with observed high response rates to immunotherapies in PI-refractory MM patients.[39] Moreover, in PI-resistant cells, we identified reduced expression of genes involved in ribonuclease H2 complex and FACT complex, which are involved in DNA repair, replication, and transcription,[40,41] suggesting that genomic instability may be linked to resistance to PIs (Figures 2H and S2F). Accordingly, analysis of upregulated phosphorylated proteins in PI-resistant cells showed enriched signatures of DDR and regulation of DNA replication and increased ATM/CHEK2/CHEK1 kinase activities (Figures 2I and S2G). Collectively, our data suggest that the heightened genomic instability of PI-resistant MM cells can confer sensitivity to CX-5461.

The combination of PIs with CX-5461 does not further enhance the anti-myeloma activity of CX-5461

The ubiquitin-proteasome system has non-proteolytic functions in mediating DNA repair and activating DDR signaling, and PIs have been shown to impair DNA repair capacity, causing HR deficiency and persistent DNA damage.[42–44] We therefore assessed whether combining CX-5461 with PIs can improve their efficacy by increasing DNA damage levels in MM cells. We examined combining CX-5461 and bortezomib in four HMCLs including p53 WT MM1.S and MOLP-8, p53 mutant cell lines OPM-2 and JJN3 (Figure 3A). Surprisingly, no synergist effects between CX-5461 and bortezomib were observed. We further examined the benefit of combining CX-5461 with carfilzomib in C57BL6/KaLwRij mice transplanted with 5T33 MM cells. While carfilzomib as a single agent showed no benefit, CX-5461 showed significant therapeutic benefit in 5T33 MM-bearing mice (Figure 3B). Consistent with our *in vitro* findings, the combination therapy did not significantly improve the survival benefit compared to CX-5461 as a single agent.

We next examined the effect of combining CX-5461 and bortezomib in inducing DDR signaling in four HMCLs (Figure 3C). In agreement with previous reports,[43] bortezomib markedly decreased the abundance of key proteins involved in ATM/ATR signaling including ATM and ATR substrate CHK1 and their phosphorylation levels. This impaired DNA repair activity is associated with accumulation of DNA damage as shown by increased γH2AX levels. Surprisingly, bortezomib effectively abrogated CX-5461-mediated ATM/ATR activation; however, γH2AX level remained the same as those induced by bortezomib alone. Our data thus suggest that bortezomib attenuates CX-5461-mediated DDR activation and that the combination therapy fails to exacerbate DNA damage and consequently does not further enhance anti-tumor action. Nevertheless, the data support that CX-5461's significant anti-MM activity in the 5T33-KalwRij model is mediated via its multiple modes of action as a dual inhibitor of Pol I transcription and TOP2 activity.

CX-5461 is synergistic with the histone deacetylase inhibitor panobinostat

We next performed a boutique screen of CX-5461 in combination with drugs with known clinical or promising preclinical efficacy in MM in 14 HMCLs and measured cell proliferation using RealTime-Glo cell viability assay. Representative dose-response curves are shown in Figure S3. Co-treatment with the histone deacetylase inhibitor (HDACi) panobinostat and CX-546 elicited the strongest combination effect in inhibiting MM cell growth (Figure S3I). Further assessment of the response to this combination therapy in four HMCLs demonstrated synergistic cell death as determined by CalcuSyn (Figures 4A and 4B).

We subsequently assessed the therapeutic benefit of CX-5461 and panobinostat using the Vκ*MYC MM model, a *MYC*-driven murine model that closely resembles the clinical and genomic features of human MM.[45,46] The combination of CX-5461 and panobinostat demonstrated significant survival benefit by comparison to single-agent treatments (Figures 4C and 4D). Disease progression measured by peripheral paraprotein levels was significantly reduced following treatment with either CX-5461 or panobinostat and further delayed by the combination treatment (Figure 4C). Mice treated with the combination therapy had a median survival of 162.5 days, compared with 131 days in mice treated with CX-5461 ($p = 0.007$), 126 days in those treated with panobinostat ($p = 0.046$), and 109 days in the vehicle-treated mice (Figure 4D). Prolonged dosing with CX-5461 and panobinostat did not cause toxicity beyond that seen with single agents, nor any significant weight loss (Figure S4A), and with only mild anemia observed (Figure S4B).

To further explore the impact of the combination treatment, we examined the benefit of combining CX-5461 with panobinostat in C57BL-KaLwRij mice transplanted with luciferase-expressing 5T33 MM cells. Serial assessment of tumor burden by bioluminescence imaging demonstrated that cancer progression was delayed in the single-agent groups, and further retarded in the combination group with markedly enhanced survival benefit (Figures 4E and 4F). Compared

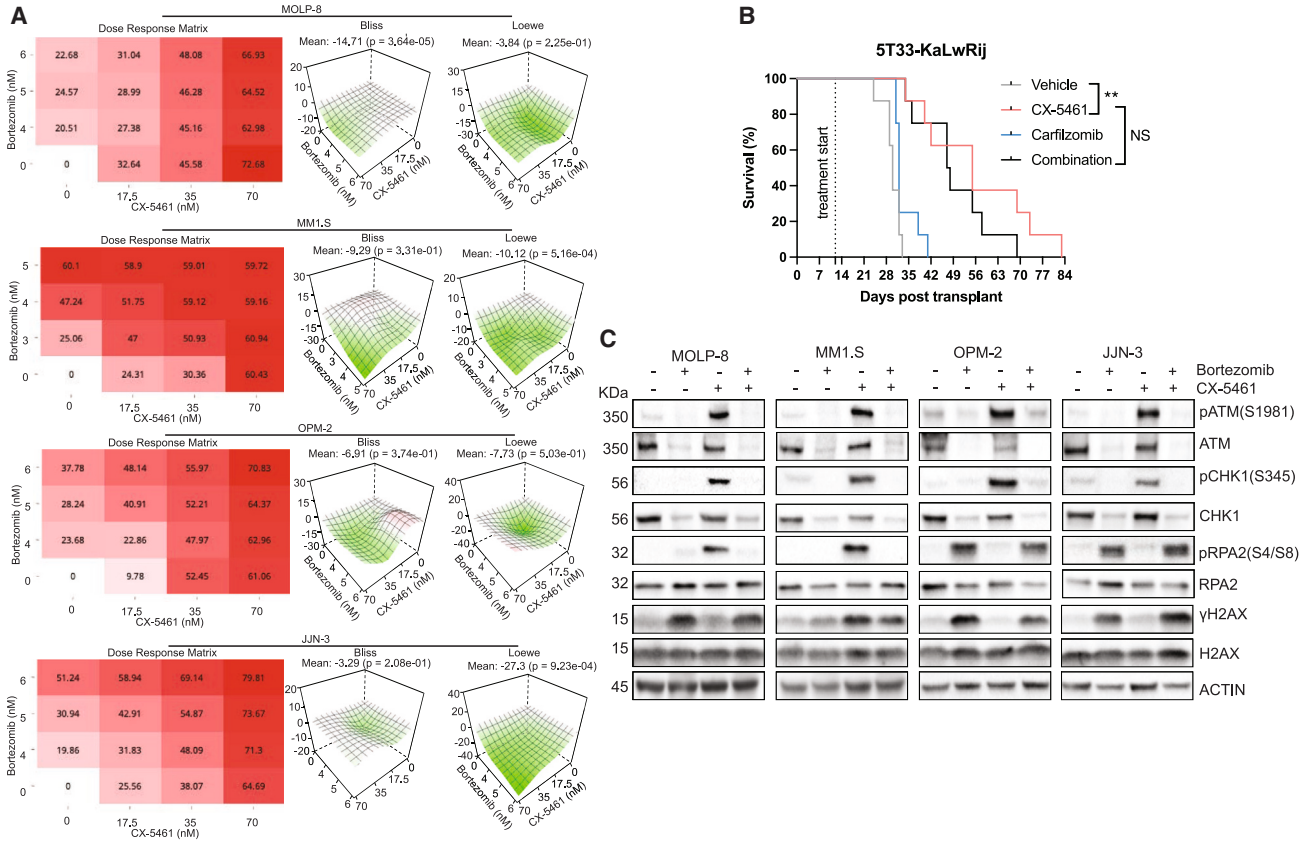

Figure 3. The combination with PIs does not further enhance the anti-myeloma activity of CX-5461

(A) Cells were treated with CX-5461 and bortezomib for 72 h and the number of viable cells were counted by Coulter Counter. The mean of n = 3 is shown in the dose-response matrix (left). The synergy scores were calculated using Bliss (middle) and Loewe (right) models on SynergyFinder Application website (SynergyFinder.com). (B) C57BL/KaLwRij mice were transplanted with 2×10^6 luciferase-expressing 5T33 MM cells by intravenous tail injection. The treatment started on day 12 post transplantation with carfilzomib 5 mg/kg i.p. injection weekly, CX-5461 25 mg/kg oral gavage three times per week, the drug combination, or the vehicle control (n = 8 per condition). A Kaplan-Meier plot is shown. Statistical analysis was performed by log rank test. **$p < 0.01$; ns, non-significant. (C) Western blotting of HMCLs treated with 5 nM bortezomib or 500 nM CX-5461 for 24 h. Actin was probed as a loading control. Representative images of n = 3.

to the vehicle-treated mice, panobinostat-treated mice survived a median of 7 days longer, the CX-5461-treated an additional 13.5 days, and the combination-treated mice 30 days longer, providing a statistically significant survival improvement in the combination-treated group compared with either panobinostat ($p = 0.001$) or CX-5461 alone ($p = 0.003$; Figure 2G) without significant weight loss (Figure S4C). Taken together, the survival benefit provided by combining CX-5461 with panobinostat in two genetically distinct MM mouse models supports the potential for this combination therapy to be applicable across clinical presentations with different genetic aberrations.

The combination of CX-5461 and panobinostat enhances MM cell death through inhibition of protein synthesis via independent pathways

To investigate the molecular mechanisms underlying the synergistic response to CX-5461 and panobinostat, we performed RNA sequencing (RNA-seq) analysis in both p53-WT MM1.S and p53-null JJN-3 cells (Figures S5A and S5B). The ssGSEA demonstrated that genes associated with apoptosis, mitotic spindle, DNA repair, and UV response were upregulated by CX-5461, consistently supporting CX-5461-mediated DDR (Figures 5A and S5C). However, these signatures were not significantly modulated in cells treated with panobinostat alone. Instead, downregulation of gene expression signatures including MYC targets and mTORC1 signaling were detected upon panobinostat treatment, consistent with the known mode of action of panobinostat in MM.[47] Interestingly, all these effects exerted by single agents were not further enhanced by the combination therapy, suggesting that the synergy is associated with distinct mechanisms of action of the two drugs. Nonetheless, we expect that these drugs in combination might have long-term effects on MM cell's transcriptome, thereby enhancing their synergy.

We thus measured ATM/ATR signaling activity and MYC protein expression by western blotting. The addition of panobinostat did not further increase pCHK2 T68, pCHK1 S345, and pRPA2 S33,

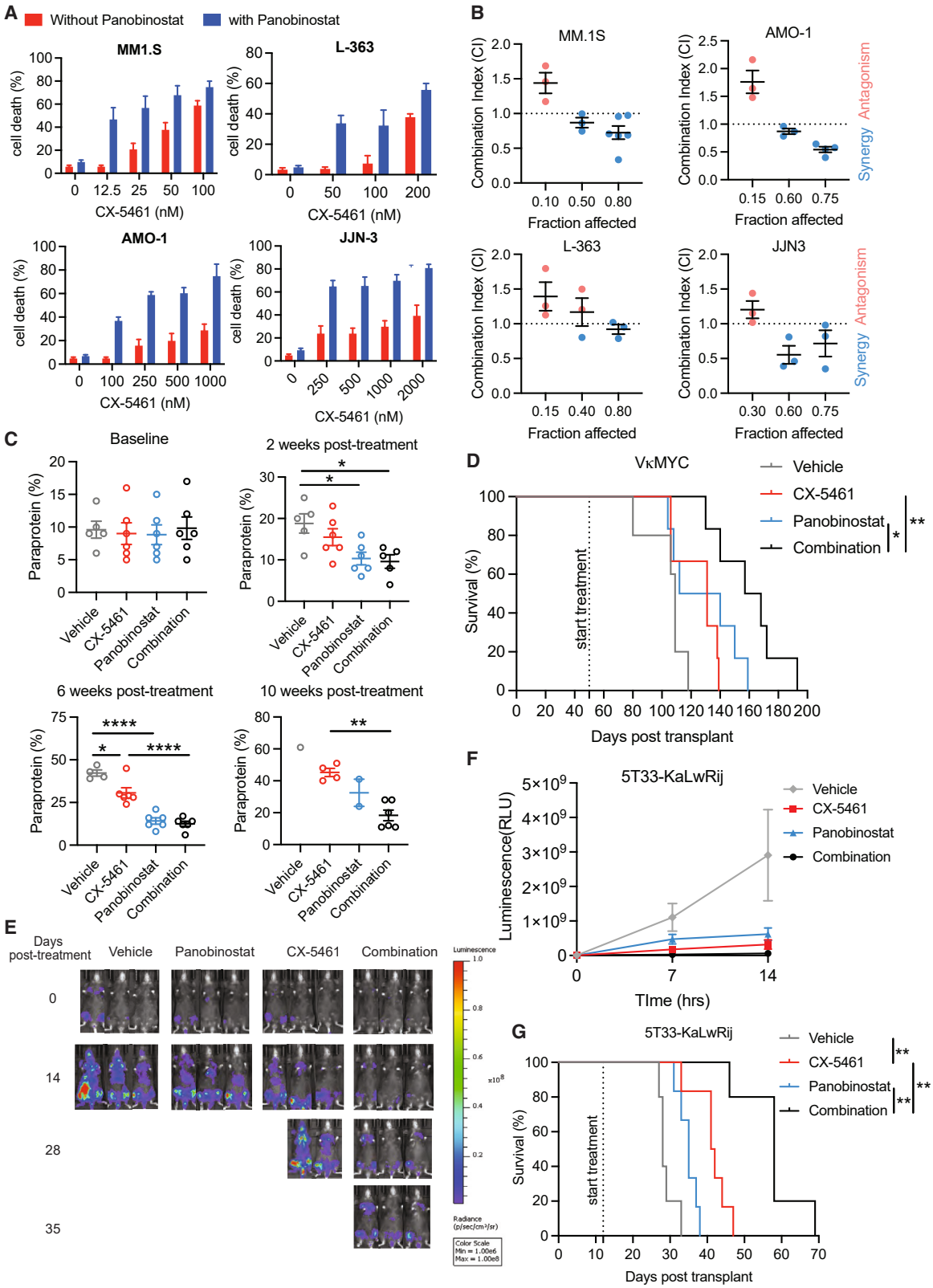

(legend on next page)

nor γH2AX levels by CX-5461, suggesting that panobinostat does not augment CX-5461-mediated DDR and replication stress (Figures 5B and 5C). While MYC expression was not significantly affected by CX-5461 treatment in either cell line, panobinostat drastically reduced MYC expression, confirming the downregulation of MYC activity identified by ssGSEA. Moreover, this effect was not enhanced by the combination treatment, further supporting that CX-5461and panobinostat inhibit MM growth via independent pathways.

Since both MYC and mTORC1 are master regulators of mRNA translation and protein synthesis, inhibition of MYC activity and mTORC1 signaling by panobinostat may impair mRNA translation, which is also a functional impact of CX-5461 (Figures 2C–2E). We thereby assessed whether the improved therapeutic efficacy of the CX-5461/panobinostat combination is a result of cooperative inhibition of protein synthesis. Measuring protein synthesis rate using AHA incorporation showed that both CX-5461 and panobinostat reduced the abundance of newly synthesized proteins in AMO-1 cells (Figure 5D). In contrast, protein synthesis rate in JJN3 cells was only reduced by panobinostat but not affected by CX-5461 (Figure 5E), in line with its lower sensitivity to CX-5461 (Figure S1B). Nevertheless, CX-5461 plus panobinostat provided enhanced inhibition of protein synthesis (Figures 5D and 5E). Taken together, our data suggest that the combination of CX-5461 and panobinostat enhances inhibition of mRNA translation and protein synthesis through independent pathways, which contribute to the synergy observed in MM cell lines and mouse models.

DISCUSSION

CX-5461 has demonstrated a promising single-agent anti-tumor activity and a safety profile in a phase I clinical study in patients with advanced hematological malignancies. A halt in disease progression was noted in 50% (three out of six) of MM patients, which in this study of heavily pre-treated patients was the best response.[23] We herein demonstrate that the dual mode of action of CX-5461 in inhibiting ribosome biogenesis and activating DDR contributes to its potent efficacy in PI-resistant MM models. Moreover, we demonstrate that the combination of CX-5461 and panobinostat is synergistic in inhibiting MM *in vitro* and *in vivo* by cooperatively suppressing mRNA translation.

The molecular response to CX-5461

CX-5461 inhibits Pol I transcription and subsequently induces the canonical nucleolar stress response via the release of free ribosomal proteins, which then bind and inhibit nucleosplasmic MDM2, a negative regulator of p53, resulting in cell-cycle arrest/apoptosis.[15] In MM cells, we observed a modest but significant correlation of *TP53* status with sensitivity to CX-5461, with *TP53* mutant HMCLs being less sensitive to CX-5461-induced cell death. Results from the clinical study of CX-5461 in hematological malignancies demonstrated that, of the four MM patients whose *TP53* status was determined by sequencing, two patients with *TP53* WT achieved stable disease for four cycles and the third patient with *TP53* WT MM and a patient with *TP53*-mutated MM experienced early disease progression.[23] Thus, whether *TP53* can serve as a predictor of CX-5461 in MM remains unclear and is worthy of further investigations.

In agreement with responses observed in AML and ovarian cancer models, CX-5461 induced the DDR in HMCLs independent of p53 status. The CX-5461 mode of action includes DNA-structure-mediated TOP2 inhibition via stabilizing G4 DNA structures[26] or R-loops,[18,20,25] which are enriched at rRNA genes. Notably, TOP2A is an essential component of the initiation-competent Pol I complex[48] and thus CX-5461 can trap TOP2A at the rRNA gene promoters and other regions across the genome leading to replication stress. While it is not yet clear how CX-5461 affects TOP2 activity, it acts differently to classical TOP2 inhibitors etoposide and doxorubicin. This is supported by the finding in ovarian cancer cells that CX-5461-mediated replication stress occurs with overall lower levels of global γH2AX, compared to doxorubicin.[19] Thus, the clinical toxicities associated with TOP2 inhibitors such as cardiotoxicity[49] are unlikely to apply to CX-5461.

Although PIs have been reported to sensitize cancer cells to various chemotherapies and radiation therapy,[50,51] co-treatment of PIs with CX-5461 did not show additive effects on the induction of DDR and cell death in MM. It is important to note that the balance between proteasome capacity and workload has been proposed to determine the sensitivity to PIs.[52] Depletion of genes involved in protein synthesis, including components of the eIF4F translation initiation complex, protected MM cells from carfilzomib-induced cell death by alleviating the load on the proteasome.[53] In this regard, CX-5461-mediated

Figure 4. CX-5461 is synergistic with the histone deacetylase inhibitor panobinostat

(A) Cells were treated with increasing concentrations of CX-5461 in the presence or absence of 50 nM panobinostat for 72 h. Cell death was assessed by propidium iodide exclusion assay. Error bars represent mean ± SEM, n = 3. (B) Combination indices (CIs) calculated by CalcuSyn software. CI < 1 indicates synergistic cell death (blue), CI > 1 indicates antagonism (red), CI = 1 indicates additive effect (black). Error bars represent mean ± SEM, n = 3. (C and D) 3.5×10^5 spleen cells from Vκ*MYC mice (clone 4929) were transplanted into C57BL/6 mice following sub-lethal irradiation. After 7 weeks, mice were randomized based on the paraprotein levels into four groups and started treatment with 35 mg/kg CX-5461 twice weekly via oral gavage (n = 6 mice), 7.5 mg/kg panobinostat via i.p. injection three times weekly (n = 6 mice), the combination of CX-5461 and panobinostat (n = 6 mice), or vehicle control (n = 5 mice). The paraprotein level is presented as the percentage of total proteins, as measured by serum protein electrophoresis at baseline, 2-week, 6-week, and 10-week time points (C). Error bars represent mean ± SEM. Statistical analysis is performed using one-way ANOVA, Tukey's multiple comparations test. *p < 0.05, ***p < 0.001, ****p < 0.0001. Kaplan-Meier plot (D). Statistical analysis is performed using log rank test. *p < 0.05, **p < 0.01. (E–G) 2×10^6 luciferase-expressing 5T33 cells were transplanted into C57BL-KaLwRij mice. Mice were randomized based on bioluminescent imaging on day 12 post transplantation into four groups and started treatment with 25 mg/kg CX-5461 via oral gavage three times weekly (n = 6 mice), 5 mg/kg panobinostat via i.p. injection three times weekly (n = 6 mice), the combination of CX-5461 and panobinostat (n = 5 mice), or vehicle control (n = 5 mice). Bioluminescent images are shown (E). Disease burden measured by bioluminescent signal intensity (photons per second) (F). Kaplan-Meier plot (G). Statistical analysis was performed using log rank test, **p < 0.01.

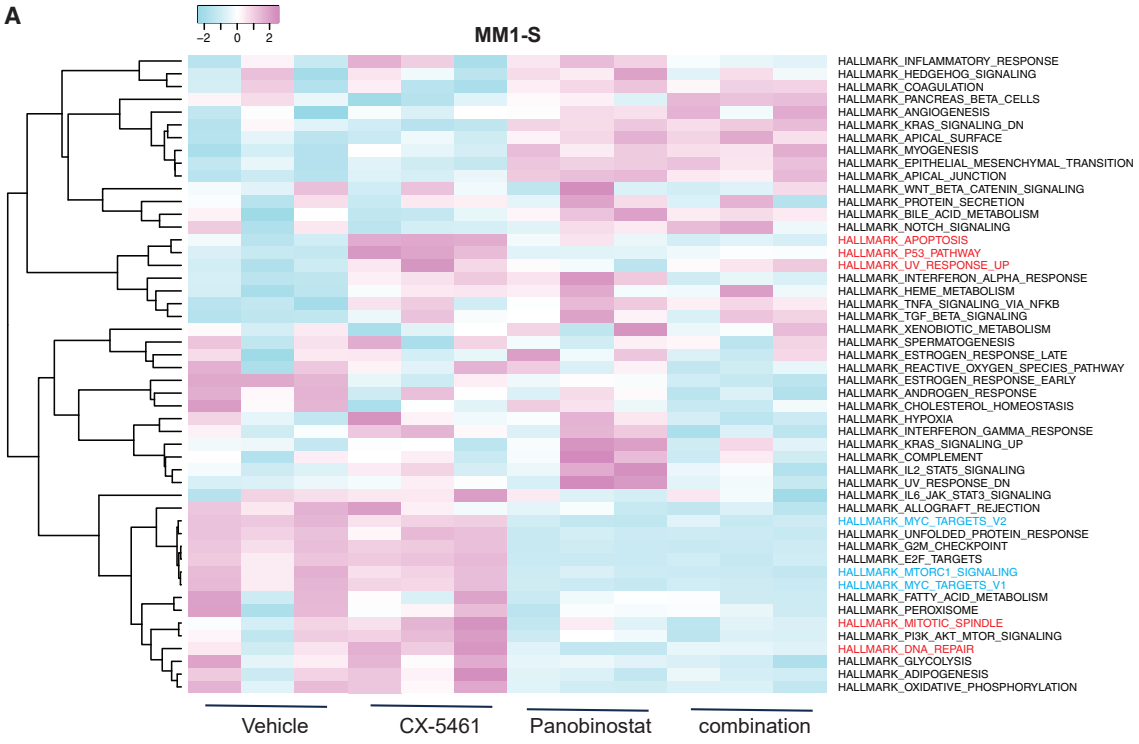

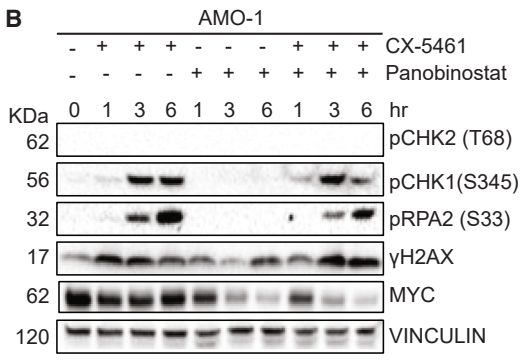

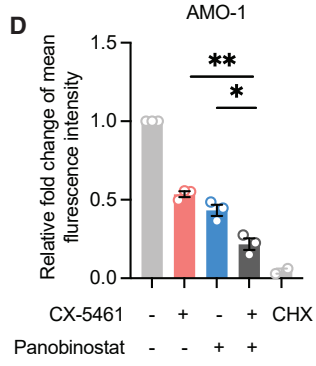

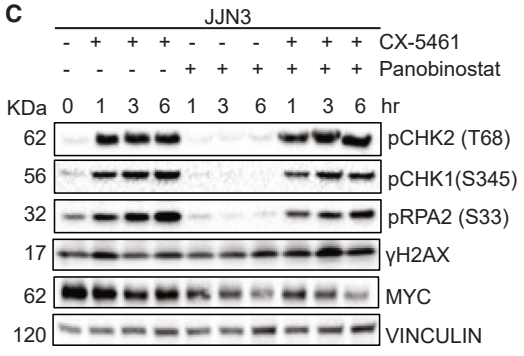

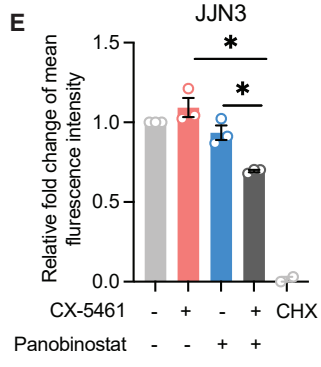

(legend on next page)

inhibition of ribosome biogenesis, and new protein synthesis could alleviate the proteasome's workload and consequently attenuate the response to proteosome inhibition.

Targeting ribosome synthesis and function as a therapeutic strategy in refractory MM

Increased ribosome biogenesis and mRNA translation are fundamentally associated with malignant transformation across multiple cancers, including MM. The transcription factor MYC plays a central role in MM progression with a strong correlation between MYC expression and translational activity in MM having been established.[54] In addition to MYC, other MM genetic drivers, for instance, *TP53* deletion and hyperactivation of the RAS pathway also have direct impacts on mRNA translational activity, potentially contributing to progression from precursor states to malignant disease. Therefore, oncogenic reprogramming of mRNA translation may drive MM pathogenesis. The high rate of protein synthesis and processing in MM leads to proteotoxic stress and may cause a heavy reliance on ribosomes and proteasomes. Disrupting the balance between protein synthesis and degradation provides a new option for treating MM. Evidence from several studies has provided a rationale for targeting mRNA translation in MM cells. Inhibiting the initiation step of protein translation by knocking down eIF4E hinders MM growth and survival.[55,56] Translational initiation inhibitors rocaglates and omacetaxine have been shown to suppress MM cell proliferation and induce cell death.[54,57] In line with these findings, we show that the combination of CX-5461 with panobinostat produced a double hit on ribosome biogenesis and mRNA translation in MM cells. Altogether, our findings support the feasibility of targeting the ribosome as an effective strategy to treat RRMM. Last, our work highlights the importance of understanding drugs' mechanisms of action and the mechanisms of drug synergy to apply a personalized/precision medicine approach in MM. This is particularly important for MM given the breadth of treatments available and the current complex therapeutic landscape.

MATERIALS AND METHODS

Cell lines

The source and culture conditions for mouse myeloma cell lines and HMCLs used in this study are listed in Table S1. The identity and individuality of HMCLs were routinely confirmed by a polymerase chain reaction (PCR)-based short tandem repeat (STR) analysis. Cells are routinely tested for mycoplasma contamination by PCR and kept in a humidified 5% CO_2 incubator at 37°C.

The mouse MM cell line 5T33 was transduced with a FUL2-TG lentivirus vector containing Luciferase-2 and eGFP genes. Resistance to the PI bortezomib in JJN3 and 5T33 MM cell lines was established by continuously maintaining the cells in culture medium supplemented with increasing drug concentrations over 6 months. The parental cell lines were maintained in culture medium supplemented with DMSO vehicle at the same concentrations as the drug-resistant cells and passaged in an identical fashion.

Compounds

For *in vitro* studies, CX-5461 was purchased from SYNkinase and MedChemExpress and dissolved in 50 mM NaH_2PO_4 (pH 4.5). Bortezomib, carfilzomib, and panobinostat were purchased from SelleckChem and prepared in DMSO. For *in vivo* studies, CX-5461 was freshly prepared in 25 mM NaH_2PO_4 (pH4.5) on the day of dosing. Bortezomib (Velcade, Celgene) and carfilzomib (Kyprolis, Amgen) were obtained from the cytotoxic pharmacy of the Peter MacCallum Cancer Centre.

Propidium iodide exclusion assay

Exponentially growing cells were seeded into 96-well plates at 20,000 cells in 100 μL per well in technical triplicate. After 24-h incubation, 100 μL of drug dilutions were added to the cell culture. At 24 or 72 h after drug treatment, propidium iodide was added for 15 min and cells analyzed by FACS-Verse flow cytometer (BD Biosciences). The data were analyzed using FlowLogic software (Inivai Technologies) and plotted using Prism GraphPad 6.0/7.0 software to calculate EC50 of cell death.

Cell-cycle analysis

Cells were labeled with 3 μM bromodeoxyuridine (BrdU) (BD Pharmigen) for 30 min then fixed with cold 80% ethanol. Cells were stored at 4°C for a maximum of 1 month. On the day of analysis, cells were resuspended in 2 N HCL with 0.5% (v/v) Triton X-100 and incubated for 30 min at room temperature (RT) followed by the addition of 0.1 M sodium tetraborate for 5 min. Anti-BrdU antibody (BD Biosciences) diluted in PBS containing 2% FBS and 0.5% Tween 20 was added at 1:50 dilution and then incubated at RT for 30 min. Cells were washed with 2% FBS in PBS, then incubated with fluorescein labeled sheep anti-mouse immunoglobulin (Ig) G (MP Biomedicals) at 1:100 dilution for 30 min at RT. Cells were then washed and resuspended in PBS containing 2% FBS and 10 μg/mL PI. The analysis was performed on the FACSVerse flow cytometer (BD Biosciences). The data were analyzed using FlowLogic software (Inivai Technologies) and plotted using Prism GraphPad 6.0/7.0 software.

Figure 5. The combination of CX-5461 and panobinostat enhances multiple myeloma cell death through inhibition of protein synthesis via independent pathways

(A) MM.1S cells were treated with vehicle, 500 nM CX-5461, 50 nM panobinostat, or the combination for 24 h and cellular RNA was extracted for 3′ RNA-seq analysis (n = 3). Changes of activities of hallmarks upon treatment were determined by single-sample GSEA using MSigDB hallmark gene sets. (B and C) AMO-1 (B) and JJN3 (C) cells were treated as in (A) and analyzed by western blotting. Vinculin was probed as a loading control. Representative images of n = 3. (D and E) AMO-1(D) and JJN-3 (C) cells were treated as in (A) for 6 h and labeled with 50 μM L-azidohomoalanine for 1 h before fixing followed by labeling with 1 μM Alexa Fluor 488-azide and flow cytometry analysis. The median fluorescence intensity was normalized to vehicle control. Error bars represent mean ± SEM, n = 3. Statistical analysis was performed using one-way ANOVA Tukey's multiple comparisons test. *$p < 0.1$, **$p < 0.01$.

Boutique drug screen to assess CX-5461 combination therapies

Exponentially growing cells were seeded into 384-well plates at 2,500 cells in 25 μL per well in technical triplicate using an automated micropipette liquid handling system (Biotek). After 24-h incubation, 10 μL of diluted Promega Real-Time Glo enzyme and substrate were added (Promega, G9712; 10 μL of each component diluted in 8 mL of medium). Drug solutions were prepared at 10× final concentration and 5 μL per well were added by ALH3000 robot (Biotek). The bioluminescence was measured at baseline (15 min after adding Real-Time Glo reagents) and every 24 h using the Cytation plate reader (BioTek). The bioluminescent values were normalized to vehicle-treated and to baseline luminescence levels. Values for inhibition of 50% of proliferation (GI50) were calculated using Prism GraphPad 6.0/7.0 software.

RADAR assay

RADAR assays were performed as described previously.[58] Briefly, cells were lysed in the lysis buffer containing 6 M guanidinium thiocyanate, 10 mM Tris-HCl, pH 6.5, 20 mM EDTA, 4% Triton X-100, 1% Sarkosyl, and 1% dithiothreitol. Nucleic acid and DNA-protein covalent complexes were then recovered by adding 100% ethanol, incubation at −20°C for 5 min and centrifugation for 15 min at 15,000 rpm. The pellet was washed twice with 75% ethanol and promptly dissolved in 8 mM NaOH. Equal amounts of DNA diluted in Tris-buffered saline (TBS) buffer (to a final volume of 200 μL) were made up in 96-well microtiter plate. The samples were then applied onto a nitrocellulose membrane using Bio-Dot SF Microfiltration Apparatus according to the manufacturer's instructions. The membrane was rinsed with TBS buffer containing 0.1% Tween 20 (TBS-T), blocked with 5% skim milk in TBS-T for 1 h and subsequently incubated with mouse anti-TOP2a antibody (SantaCruz, Sc-166934, 1:1,000 dilution) at 4°C overnight. Following three 5-min washes with TBS-T, the membrane was incubated with LI-COR IRDye 800CW goat anti-mouse IgG Secondary Antibody (0.5 mg, LI-COR 92632210) and imaged on the LI-COR Odyssey CLx (LI-COR Biosciences).

qRT-PCR

Total RNA was extracted according to the NucleoSpin RNA extraction kit protocol (Mecherey-Nagel). An equal amount of total RNA was treated with DNase at 37°C for 15 min followed by 65°C for 15 min. cDNA was synthesized as per the SuperScript III kit (Life Technologies) using random hexamer primers (Promega). qRT-PCR analysis was performed on the StepOne Plus System (Applied Biosystems) using FAST SYBR green (Applied Biosystems). The expression of target genes was normalized to *β-2-microglobulin* (*B2M*) and compared to the vehicle control. The primer sequences are detailed in Table S5.

AHA labeling

Cells are labeled with 50 μM Click-IT AHA (Thermo Fisher C10102) in methionine-free medium for 1 h. The fixed cells were incubated with click reaction mixture (50 mM Tris-HCl pH 8.0, 1 μM Alexa Fluor 488-azide [Thermo Fisher A10266], 2 mM copper sulfate [Sigma C1297], 100 mM sodium ascorbate [Sigma A4034]) for 30 min at RT. Samples were analyzed by FACSVerse flow cytometer (BD Biosciences). Data were analyzed using FlowJo software.

Western blotting

Protein lysates were extracted in the SDS-lysis buffer (0.5 mM EDTA, 20 mM HEPES, 2% (w/v) SDS pH 7.9). Samples were boiled to 95°C for 5 min and DNA was sheared using a 26G needle before being stored at −20°C for further processing. Equal amounts of protein lysates (10–30 μg) were loaded into 4%–15% precast gels (Bio-Rad) and ran using sodium dodecyl sulfate polyacrylamide gel electrophoresis (SDS-PAGE) in Tris-glycine-SDS running buffer. Separated proteins were then transferred onto Immobilon-P polyvinylidene difluoride (PVDF) membrane (Millipore IPVH00010) using the Mini-PROTEAN III system (Bio-Rad). After transfer, membranes were blocked with 5% milk in TBS-T blocking buffer at RT for 1 h and then incubated with primary antibodies diluted in blocking buffer at 4°C overnight. The following morning, the membranes were washed three times with TBS-T then incubated with mouse or rabbit horseradish peroxide-bound secondary antibodies followed by three washes with TBS-T. The protein was visualized using the Western Lighting Plus ECL kit (PerkinElmer). Images were acquired using ChemiDoc Touch system (Bio-Rad) and processed by Image Lab software (Bio-Rad). The primary and secondary antibodies are listed in Table S2.

Immunofluorescence

Exponentially growing cells were labeled with 10 μM EdU for 30 min prior to treatment. Cells were then fixed with 2% paraformaldehyde (ProSciTech) in PBS at RT for 5 min and washed with PBS. Cells were then spun onto SuperFrost Plus microscope slides (Fisherbrand) using a Shandon Cytospin 4 (Thermo Scientific) for 7 min at 800 rpm and stored at −20°C. Fixed cells were permeabilized with 0.3% (v/v) Triton X-100 in PBS for 10 min on ice, washed three times in PBS, and blocked in 5% (v/v) goat serum with 0.3% Triton X-100 in PBS at RT for 30 min. Cells were subsequently incubated with primary antibodies (Table S2) diluted in 1% (w/v) BSA with 0.3% Triton X-100 in PBS at 37°C for 1 h. After incubation, slides were washed three times in PBS. Cells were then stained with secondary antibodies diluted in 1% (w/v) BSA with 0.3% Triton X-100 in PBS at 37°C for 1 h. Slides were again washed three times in PBS (protected from light). To distinguish replicating cells in S-phase, cells were incubated with click reaction mixture (100 mM Tris [pH 8.5], 100 mM ascorbic acid, 1 mM $CuSO_4$, 10 μM Click-iTTM EdU Alexa Fluor 647 Azide; Invitrogen #A10277) at RT for 30 min and washed twice in PBS (protected from light). To counterstain the nuclei, cells were incubated with 4′,6-diamidino-2-phenylindole (DAPI) diluted 1:10,000 in PBS. Slides were finally mounted with ProLong Gold Antifade. Immunofluorescence was visualized with a Stellaris 5 confocal microscope (Leica Microsystems). Images were processed and analyzed by Fiji and Cell-Profiler Software.

Proteomics and phosphoproteomics

Sample preparation

Cells were lysed with guanidium chloride lysis buffer containing 6 M guanidinium chloride, 100 mM Tris pH 8.5, 10 mM

tris(2-carboxyethyl)phosphine (TCEP), and 40 mM 2-chloroacetamide. Samples were boiled at 95°C for 10 min and sheared with 26G needles.

For proteomics studies, 100 μg of proteins in 200-μL volume was precipitated in the presence of 1 mL of acetone and 300 μL of methanol at −20°C overnight. The protein precipitates were washed twice with 80% (v/v) acetone at −20°C and resuspended in 50 mM Tris-HCl pH 8. Then 20 μg of each protein sample was digested by Trypsin/Lys-C Mix, Mass Spec Grade (Promega, V5071) at 1:50 enzyme-to-protein ratio at 37°C, 1,000 rpm overnight. Protein samples were desalted using home-made C18 tips and eluted with 60% (v/v) acetonitrile and 5% (v/v) formic acid. After speed vacuum evaporation, proteins were resuspended in 20 μL of 1% (v/v) formic acid and subject to liquid chromatography (LC)-mass spectrometry (MS) analysis.

For phosphoproteomic studies, 300 μg of proteins in 200-μL volume was precipitated, washed, and digested by Trypsin/Lys-C Mix as described above. The phosphorylated peptides were enriched using the PureCube Fe(III)-nitrilotriacetate (NTA) MagBeads (Cube Biotech, catalog no. 31501-Fe) by rotating at RT for 1 h, according to the manufacturer's protocols. Fe(III)-NTA MagBeads bound to phosphopeptides were separated from the supernatant on a magnetic rack. Phosphopeptides were washed with 80% (v/v) acetonitrile and 0.1% (v/v) trifluoroacetic acid, then eluted with 50% (v/v) acetonitrile and 2.5% (v/v) ammonium hydroxide (Sigma 338818) through home-made C8 stage tips. Organic solvents were removed by speed vacuum evaporation. Samples were resuspended in 5% (v/v) formic acid, desalted using C18 tips, and eluted with 60% (v/v) acetonitrile and 5% (v/v) formic acid. After speed vacuum evaporation, samples were resuspended in 15 μL of 1% (v/v) formic acid and subject to LC-MS analysis.

LC-MS analysis

Peptide mixtures were analyzed by nanoLC-tandem MS (MS/MS) using the Q Exactive Plus Orbitrap Mass Spectrometer (Thermo Scientific) for proteomics analysis and the Orbitrap Exploris 480 mass spectrometer (Thermo Scientific) for phosphoproteomics analysis. The LC system was equipped with an Acclaim Pepmap nano-trap column (Dinoex-C18, 100 Å, 75 μm × 2 cm) and an Acclaim Pepmap RSLC analytical column (Dinoex-C18, 100 Å, 75 μm × 50 cm). The tryptic peptides were injected to the enrichment column at an isocratic flow of 5 μL/min of 2% v/v CH_3CN containing 0.1% v/v formic acid for 5 min applied before the enrichment column was switched in line with the analytical column. The eluents were 5% DMSO in 0.1% v/v formic acid (solvent A) and 5% DMSO in 100% v/v CH_3CN and 0.1% v/v formic acid (solvent B). The flow gradient was (1) 0–6 min at 3% B, (2) 6–95 min, 3%–22% B, (3) 95–105 min 22%–40% B, (4) 105–110 min, 40%–80% B, (5) 110–115 min, 80%–80% B, and (6) 115–117 min, 80%–3% and equilibrated at 3% B for 10 min before the next sample injection.

For samples run on the Q Exactive Plus Orbitrap, the mass spectrometer was operated in the data-dependent mode, whereby full MS1 spectra were acquired in positive mode, 70,000 resolution, AGC target of $3e^6$, and maximum IT time of 50 ms. Fifteen of the most intense peptide ions with charge states ≥ 2 and intensity threshold of $1.7e^4$ were isolated for MS/MS. The isolation window was set at 1.2 *m/z* and precursors fragmented using normalized collision energy of 30, 17,500 resolution, AGC target of $1e^5$, and maximum IT time of 100 ms. Dynamic exclusion was set to be 30 s.

For samples analyzed on the Obritrap Exploris, the mass spectrometer was operated in the data-dependent acquisition mode, whereby full MS1 spectra were acquired in a positive mode at 120,000 resolution. The top-speed acquisition mode with 3-s cycle time on the most intense precursor ion was used, whereby ions with charge states of 2–7 were selected. MS/MS analyses were performed by 1.6 *m/z* isolation with the quadrupole, fragmented by HCD with collision energy of 30%. MS2 resolution was at 15,000. Dynamic exclusion was activated for 30 s. AGC target was set to standard with auto maximum injection mode. Dynamic exclusion was activated for 30 s. All the studies were conducted at the Mass Spectrometry and Proteomics Facility, Bio21 Molecular Science and Biotechnology Institute, Melbourne, Australia as previously described.[59]

Data analysis

Raw files were processed using MaxQuant (version 2.0.3.0) with the Andromeda search engine for protein and peptide identification.[60] The results were searched against a *Mus musculus* database (SwissProt, Taxonomy ID 10090, downloaded August 2022) and using the default search parameters. Trypsin was selected as the cleavage enzyme, and cysteine carbamidomethyl was selected as fixed modification. Proteomics analysis selected methionine oxidation as variable modification. Phosphoproteomics analysis selected methionine oxidation, serine, threonine, and tyrosine phosphorylation as variable modifications. The match between run option was selected. The processed data were analyzed with Perseus (version 1.6.15.0).

For proteomics analysis, the "contaminants", "reverse" and "only identified by site peptides" were removed from the matrix. The data were log2 transformed and filtered by valid values with a minimum of three valid values in each group. The intensities of peptides in each sample were normalized by subtracting the median and missing values were imputed from normal distribution (0.3 width, 1.8 down shift). A total of 2,628 proteins were selected for statistical analysis. The significantly expressed proteins were identified by Student's t tests, defined by p value ≤ 0.05 and absolute fold change ≥ 1.5.

For phosphoproteomics analysis, the "contaminants", "reverse" and "only identified by site peptides" were removed from the matrix. Peptides with phosphate localization probability higher than 0.75 were used for further analysis. After expanding the site table, phosphopeptides intensities were log2 transformed and filtered by valid values with a minimum of three valid values in each group. The intensities of phosphopeptides in each sample were normalized by subtracting the median and imputing missing values from normal distribution (0.3 width, 1.8 down shift). A total of 4,253 phosphor sites were

selected for further statistical analysis. The significantly phosphorylated proteins were identified by Student's t tests, defined by p value ≤ 0.05 and absolute fold change ≥ 2.0.

Gene Ontology and pathway analysis were performed with STRING (version 11.5).[61] For phosphoproteomics analysis, the substrate-kinase relationships were searched using a combination of KEA3 App[37] and Phosphomatics (version 2 beta)[38] to determine the upstream kinases responsible for significantly changed phosphor-sites.

RNA-seq

RNA samples were extracted using the RNeasy Mini Kit (Qiagen, 74106) and TruSeq RNA (Illumina, catalog no. RS-122-2001) was used for sample preparation. Single-ended 75-bp RNA-seq on Illumina NextSeq 500 was performed.

FASTQ files were uploaded to Galaxy Australia (version 21.09). Quality control was performed on all samples using FastQC (version 0.73) and MultiQC (version 1.11). The 3′ Illumina adapter sequences were trimmed using Cutadapt (version 3.5). Sequencing reads were then aligned to the reference genome (hg19/GRCh37) using HISAT2 (version 2.2.1), and the number of reads mapped to genes was counted using featureCounts (version 2.0.1). Absolute gene expression was defined determining RPKM. Differential expression analysis was performed using limma-voom (version 3.50.0). The differentially regulated genes were filtered by an adjusted p value of 5% and a fold change of at least 1.5 and then subjected to gene set enrichment analysis (GSEA, version 4.1). Comparison of hallmark activity after treatment with either single agents or combination therapy was performed by single-sample GSEA (ssGSEA) with standard method implemented in GSVA.

Animal studies

All animal studies were approved by the Animal Experimentation Ethics Committee of the Peter MacCallum Cancer Centre (ethics number E626). The ethical endpoint was defined as the time point when mice show either early hindlimb paralysis, 20% weight loss, or general debility (hunched, ruffled, or reduced mobility). Once endpoint was reached, mice were culled by cervical dislocation or CO_2 intoxication.

*The Vκ*MYC model of MM*

The Vκ*MYC mouse model (clone #4929) was provided by Professor Ricky Johnstone at Peter MacCallum Cancer Centre, Australia, and a tumor bank was established by transplanting these cells into C57BL/6 recipient mice, aged 6–10 weeks. Mice were irradiated 1 day prior to transplantation to improve engraftment (3 Gy, 6 h apart) and given access to Ensure dietary supplement following irradiation. Cells were defrosted, washed, resuspended in sterile PBS, and injected via the tail vein. When early hindlimb paralysis developed, bone marrow and spleen were harvested and stored for future experiments.

To assess drug efficacy *in vivo*, the banked bone marrow or spleen cells were thawed, washed and resuspended in sterile PBS, counted with trypan blue, and injected into mice via the tail vein. Recipients were female C57BL/6 mice, aged 6–8 weeks, who had received two doses of pre-transplant irradiation. Disease-bearing mice were randomized into four groups based on the level of the paraprotein detected for treatment until the development of an ethical endpoint. CX-5461 was administered weekly via oral gavage and panobinostat was administered by intraperitoneal (i.p.) injection. Control mice received the equivalent volume of drug vehicles. Disease burden was monitored via measuring the paraprotein level in peripheral blood through serum protein electrophoresis (Hydasys 2 Scan, Sebia).

The 5T33-C57BL/KaLwRij model of MM

The 5T33 cells were provided by Professor Ricky Johnstone at Peter MacCallum Cancer Centre, Australia. C57BL/KaLwRij breeding pairs to establish a colony were provided by both Professor Zannettino (Centre for Cancer Biology, Adelaide, Australia) and Dr Khong (Australian Centre for Blood Diseases, Melbourne, Australia). Cells were grown *in vitro* for a maximum of 2 weeks, then counted using the Z2 Coulter Counter prior to transplantation by intravenous tail vein injection. Transplant recipients were syngeneic C57BL/KaLwRij mice (female, aged 8–12 weeks). Disease burden was assessed by bioluminescence imaging. Mice were injected with 200 μL of 15 mg/mL D-luciferin (Promega ViviGlo) via i.p. injection 5 min prior to imaging with the IVIS100 bioluminescence imaging system (PerkinElmer). Drug treatment commenced 12–14 days post transplantation. Mice were randomized to groups based on their bioluminescent signal. Mice were treated until the development of an ethical endpoint.

To assess the effectiveness of combination therapy of CX-5461 and carfilzomib, mice were irradiated, transplanted with cells, and randomized based on bioluminescent signal. Mice were treated with 5 mg/kg carfilzomib by i.p. injection weekly, 35 mg/kg CX-5461 by oral gavage twice weekly (Tuesday and Friday), or an equal volume of the vehicle control.

For the bortezomib-resistant 5T33 mouse model, cells were grown *in vitro* for a maximum of 2 weeks prior to injection. To improve and standardize tumor engraftment, mice in this model were irradiated 1 day prior to transplantation (3 Gy, 6 h apart). Following irradiation, mice were given access to Ensure dietary supplement and randomized based on bioluminescent signal at 7 days post transplant and treated with 0.7 mg/kg bortezomib by i.p. injection weekly or an equal volume of the vehicle control.

DATA AND CODE AVAILABILITY

RNA-seq data is available in NCBI GEO GSE255898. All raw data are available upon request.

SUPPLEMENTAL INFORMATION

Supplemental information can be found online at https://doi.org/10.1016/j.omton.2024.200771.

ACKNOWLEDGMENTS

This research was funded by Cancer Council Victoria (project grant#1184873), Tour de Cure Foundation, and the Barrie Dalgleish Centre for Myeloma and Related Blood Cancers. K.H.M. was supported by PhD grants from Leukaemia Foundation of Australia, the Royal Australasian College of Physicians, the Royal College of Pathologists of Australasia, the Multiple Myeloma Research Foundation, the American Society of Hematology, and the International Myeloma Society. E.S. received support from the Victorian Cancer Agency (Research Fellowship MCRF19007). J.K. received support from the 5Point Foundation (Christine Martin Fellowship).

AUTHOR CONTRIBUTIONS

K.H.M., conceptualization, data curation, formal analysis, methodology, validation, and writing draft; K.G., data curation, formal analysis, methodology, validation, and writing draft; J.K., conceptualization, data curation, formal analysis, methodology, validation, writing draft, supervision, and funding acquisition; A.C., conceptualization, data curation, and methodology; Y.C., data curation, formal analysis, methodology, and validation; N.H., conceptualization and methodology; C.C., N.B., and C.-S.A., methodology and supervision; R.B.P., A.K., E.S., R.D.H., G.P., and S.J.H., conceptualization, funding acquisition, project administration, supervision, and writing draft.

DECLARATION OF INTERESTS

R.D.H. is a Chief Scientific Advisor to Pimera, Inc.

REFERENCES

1. Cowan, A.J., Green, D.J., Kwok, M., Lee, S., Coffey, D.G., Holmberg, L.A., Tuazon, S., Gopal, A.K., and Libby, E.N. (2022). Diagnosis and Management of Multiple Myeloma: A Review. JAMA *327*, 464–477. https://doi.org/10.1001/jama.2022.0003.

2. Rajkumar, S.V., Dimopoulos, M.A., Palumbo, A., Blade, J., Merlini, G., Mateos, M.V., Kumar, S., Hillengass, J., Kastritis, E., Richardson, P., et al. (2014). International Myeloma Working Group updated criteria for the diagnosis of multiple myeloma. Lancet Oncol. *15*, e538–e548. https://doi.org/10.1016/s1470-2045(14)70442-5.

3. Gonzalez-Santamarta, M., Quinet, G., Reyes-Garau, D., Sola, B., Roué, G., and Rodriguez, M.S. (2020). Resistance to the Proteasome Inhibitors: Lessons from Multiple Myeloma and Mantle Cell Lymphoma. Adv. Exp. Med. Biol. *1233*, 153–174. https://doi.org/10.1007/978-3-030-38266-7_6.

4. Callander, N.S., Baljevic, M., Adekola, K., Anderson, L.D., Campagnaro, E., Castillo, J.J., Costello, C., Devarakonda, S., Elsedawy, N., Faiman, M., et al. (2022). NCCN Guidelines® Insights: Multiple Myeloma, Version 3.2022. J. Natl. Compr. Canc. Netw. *20*, 8–19. https://doi.org/10.6004/jnccn.2022.0002.

5. Wallington-Beddoe, C.T., Sobieraj-Teague, M., Kuss, B.J., and Pitson, S.M. (2018). Resistance to proteasome inhibitors and other targeted therapies in myeloma. Br. J. Haematol. *182*, 11–28. https://doi.org/10.1111/bjh.15210.

6. Wang, G., Fan, F., Sun, C., and Hu, Y. (2022). Looking into Endoplasmic Reticulum Stress: The Key to Drug-Resistance of Multiple Myeloma? Cancers *14*, 5340.

7. Jung, S.-H., Park, S.-S., Lim, J.-Y., Sohn, S.Y., Kim, N.Y., Kim, D., Lee, S.H., Chung, Y.-J., and Min, C.-K. (2022). Single-cell analysis of multiple myelomas refines the molecular features of bortezomib treatment responsiveness. Exp. Mol. Med. *54*, 1967–1978. https://doi.org/10.1038/s12276-022-00884-z.

8. Kang, J., Brajanovski, N., Chan, K.T., Xuan, J., Pearson, R.B., and Sanij, E. (2021). Ribosomal proteins and human diseases: molecular mechanisms and targeted therapy. Signal Transduct. Target. Ther. *6*, 323. https://doi.org/10.1038/s41392-021-00728-8.

9. van Riggelen, J., Yetil, A., and Felsher, D.W. (2010). MYC as a regulator of ribosome biogenesis and protein synthesis. Nat. Rev. Cancer *10*, 301–309. https://doi.org/10.1038/nrc2819.

10. Yang, M., Lu, Y., Piao, W., and Jin, H. (2022). The Translational Regulation in mTOR Pathway. Biomolecules *12*, 802. https://doi.org/10.3390/biom12060802.

11. Roux, P.P., and Topisirovic, I. (2018). Signaling Pathways Involved in the Regulation of mRNA Translation. Mol. Cell Biol. *38*, e00070-18. https://doi.org/10.1128/mcb.00070-18.

12. Devlin, J.R., Hannan, K.M., Hein, N., Cullinane, C., Kusnadi, E., Ng, P.Y., George, A.J., Shortt, J., Bywater, M.J., Poortinga, G., et al. (2016). Combination Therapy Targeting Ribosome Biogenesis and mRNA Translation Synergistically Extends Survival in MYC-Driven Lymphoma. Cancer Discov. *6*, 59–70. https://doi.org/10.1158/2159-8290.CD-14-0673.

13. Kusnadi, E.P., Trigos, A.S., Cullinane, C., Goode, D.L., Larsson, O., Devlin, J.R., Chan, K.T., De Souza, D.P., McConville, M.J., McArthur, G.A., et al. (2020). Reprogrammed mRNA translation drives resistance to therapeutic targeting of ribosome biogenesis. EMBO J. *39*, e105111. https://doi.org/10.15252/embj.2020105111.

14. Hein, N., Cameron, D.P., Hannan, K.M., Nguyen, N.Y.N., Fong, C.Y., Sornkom, J., Wall, M., Pavy, M., Cullinane, C., Diesch, J., et al. (2017). Inhibition of Pol I transcription treats murine and human AML by targeting the leukemia-initiating cell population. Blood *129*, 2882–2895. https://doi.org/10.1182/blood-2016-05-718171.

15. Bywater, M.J., Poortinga, G., Sanij, E., Hein, N., Peck, A., Cullinane, C., Wall, M., Cluse, L., Drygin, D., Anderes, K., et al. (2012). Inhibition of RNA polymerase I as a therapeutic strategy to promote cancer-specific activation of p53. Cancer Cell *22*, 51–65. https://doi.org/10.1016/j.ccr.2012.05.019.

16. Lawrence, M.G., Porter, L.H., Choo, N., Pook, D., Grummet, J.P., Pezaro, C.J., Sandhu, S., Ramm, S., Luu, J., Bakshi, A., et al. (2021). CX-5461 Sensitizes DNA Damage Repair-proficient Castrate-resistant Prostate Cancer to PARP Inhibition. Mol. Cancer Ther. *20*, 2140–2150. https://doi.org/10.1158/1535-7163.MCT-20-0932.

17. Rebello, R.J., Kusnadi, E., Cameron, D.P., Pearson, H.B., Lesmana, A., Devlin, J.R., Drygin, D., Clark, A.K., Porter, L., Pedersen, J., et al. (2016). The Dual Inhibition of RNA Pol I Transcription and PIM Kinase as a New Therapeutic Approach to Treat Advanced Prostate Cancer. Clin. Cancer Res. *22*, 5539–5552. https://doi.org/10.1158/1078-0432.CCR-16-0124.

18. Sanij, E., Hannan, K.M., Xuan, J., Yan, S., Ahern, J.E., Trigos, A.S., Brajanovski, N., Son, J., Chan, K.T., Kondrashova, O., et al. (2020). CX-5461 activates the DNA damage response and demonstrates therapeutic efficacy in high-grade serous ovarian cancer. Nat. Commun. *11*, 2641. https://doi.org/10.1038/s41467-020-16393-4.

19. Yan, S., Xuan, J., Brajanovski, N., Tancock, M.R.C., Madhamshettiwar, P.B., Simpson, K.J., Ellis, S., Kang, J., Cullinane, C., Sheppard, K.E., et al. (2021). The RNA polymerase I transcription inhibitor CX-5461 cooperates with topoisomerase 1 inhibition by enhancing the DNA damage response in homologous recombination-proficient high-grade serous ovarian cancer. Br. J. Cancer *124*, 616–627. https://doi.org/10.1038/s41416-020-01158-z.

20. Pan, M., Wright, W.C., Chapple, R.H., Zubair, A., Sandhu, M., Batchelder, J.E., Huddle, B.C., Low, J., Blankenship, K.B., Wang, Y., et al. (2021). The chemotherapeutic CX-5461 primarily targets TOP2B and exhibits selective activity in high-risk neuroblastoma. Nat. Commun. *12*, 6468. https://doi.org/10.1038/s41467-021-26640-x.

21. Negi, S.S., and Brown, P. (2015). rRNA synthesis inhibitor, CX-5461, activates ATM/ATR pathway in acute lymphoblastic leukemia, arrests cells in G2 phase and induces apoptosis. Oncotarget *6*, 18094–18104. https://doi.org/10.18632/oncotarget.4093.

22. Lee, H.C., Wang, H., Baladandayuthapani, V., Lin, H., He, J., Jones, R.J., Kuiatse, I., Gu, D., Wang, Z., Ma, W., et al. (2017). RNA Polymerase I Inhibition with CX-5461 as a Novel Therapeutic Strategy to Target MYC in Multiple Myeloma. Br. J. Haematol. *177*, 80–94. https://doi.org/10.1111/bjh.14525.

23. Khot, A., Brajanovski, N., Cameron, D.P., Hein, N., Maclachlan, K.H., Sanij, E., Lim, J., Soong, J., Link, E., Blombery, P., et al. (2019). First-in-Human RNA Polymerase I Transcription Inhibitor CX-5461 in Patients with Advanced Hematologic Cancers: Results of a Phase I Dose-Escalation Study. Cancer Discov. *9*, 1036–1049. https://doi.org/10.1158/2159-8290.CD-18-1455.

24. Hilton, J., Gelmon, K., Bedard, P.L., Tu, D., Xu, H., Tinker, A.V., Goodwin, R., Laurie, S.A., Jonker, D., Hansen, A.R., et al. (2022). Results of the phase I CCTG IND.231 trial

of CX-5461 in patients with advanced solid tumors enriched for DNA-repair deficiencies. Nat. Commun. *13*, 3607. https://doi.org/10.1038/s41467-022-31199-2.

25. Bruno, P.M., Lu, M., Dennis, K.A., Inam, H., Moore, C.J., Sheehe, J., Elledge, S.J., Hemann, M.T., and Pritchard, J.R. (2020). The primary mechanism of cytotoxicity of the chemotherapeutic agent CX-5461 is topoisomerase II poisoning. Proc. Natl. Acad. Sci. USA *117*, 4053–4060. https://doi.org/10.1073/pnas.1921649117.

26. Xu, H., Di Antonio, M., McKinney, S., Mathew, V., Ho, B., O'Neil, N.J., Santos, N.D., Silvester, J., Wei, V., Garcia, J., et al. (2017). CX-5461 is a DNA G-quadruplex stabilizer with selective lethality in BRCA1/2 deficient tumours. Nat. Commun. *8*, 14432. https://doi.org/10.1038/ncomms14432.

27. Quin, J., Chan, K.T., Devlin, J.R., Cameron, D.P., Diesch, J., Cullinane, C., Ahern, J., Khot, A., Hein, N., George, A.J., et al. (2016). Inhibition of RNA polymerase I transcription initiation by CX-5461 activates non-canonical ATM/ATR signaling. Oncotarget *7*, 49800–49818. https://doi.org/10.18632/oncotarget.10452.

28. Drygin, D., Lin, A., Bliesath, J., Ho, C.B., O'Brien, S.E., Proffitt, C., Omori, M., Haddach, M., Schwaebe, M.K., Siddiqui-Jain, A., et al. (2011). Targeting RNA polymerase I with an oral small molecule CX-5461 inhibits ribosomal RNA synthesis and solid tumor growth. Cancer Res. *71*, 1418–1430. https://doi.org/10.1158/0008-5472.CAN-10-1728.

29. Ide, S., Imai, R., Ochi, H., and Maeshima, K. (2020). Transcriptional suppression of ribosomal DNA with phase separation. Sci. Adv. *6*, eabb5953. https://doi.org/10.1126/sciadv.abb5953.

30. Mars, J.C., Tremblay, M.G., Valere, M., Sibai, D.S., Sabourin-Felix, M., Lessard, F., and Moss, T. (2020). The chemotherapeutic agent CX-5461 irreversibly blocks RNA polymerase I initiation and promoter release to cause nucleolar disruption, DNA damage and cell inviability. NAR Cancer *2*, zcaa032. https://doi.org/10.1093/narcan/zcaa032.

31. Pelletier, J., Thomas, G., and Volarević, S. (2018). Ribosome biogenesis in cancer: new players and therapeutic avenues. Nat. Rev. Cancer *18*, 51–63. https://doi.org/10.1038/nrc.2017.104.

32. Snyers, L., Laffer, S., Löhnert, R., Weipoltshammer, K., and Schöfer, C. (2022). CX-5461 causes nucleolar compaction, alteration of peri- and intranucleolar chromatin arrangement, an increase in both heterochromatin and DNA damage response. Sci. Rep. *12*, 13972. https://doi.org/10.1038/s41598-022-17923-4.

33. Son, J., Hannan, K.M., Poortinga, G., Hein, N., Cameron, D.P., Ganley, A.R.D., Sheppard, K.E., Pearson, R.B., Hannan, R.D., and Sanij, E. (2020). rDNA Chromatin Activity Status as a Biomarker of Sensitivity to the RNA Polymerase I Transcription Inhibitor CX-5461. Front. Cell Dev. Biol. *8*, 568. https://doi.org/10.3389/fcell.2020.00568.

34. Bossaert, M., Pipier, A., Riou, J.F., Noirot, C., Nguyên, L.T., Serre, R.F., Bouchez, O., Defrancq, E., Calsou, P., Britton, S., and Gomez, D. (2021). Transcription-associated topoisomerase 2α (TOP2A) activity is a major effector of cytotoxicity induced by G-quadruplex ligands. Elife *10*, e65184. https://doi.org/10.7554/eLife.65184.

35. Amend, S.R., Wilson, W.C., Chu, L., Lu, L., Liu, P., Serie, D., Su, X., Xu, Y., Wang, D., Gramolini, A., et al. (2015). Whole Genome Sequence of Multiple Myeloma-Prone C57BL/KaLwRij Mouse Strain Suggests the Origin of Disease Involves Multiple Cell Types. PLoS One *10*, e0127828. https://doi.org/10.1371/journal.pone.0127828.

36. Vanderkerken, K., De Raeve, H., Goes, E., Van Meirvenne, S., Radl, J., Van Riet, I., Thielemans, K., and Van Camp, B. (1997). Organ involvement and phenotypic adhesion profile of 5T2 and 5T33 myeloma cells in the C57BL/KaLwRij mouse. Br. J. Cancer *76*, 451–460. https://doi.org/10.1038/bjc.1997.409.

37. Kuleshov, M.V., Xie, Z., London, A.B.K., Yang, J., Evangelista, J.E., Lachmann, A., Shu, I., Torre, D., and Ma'ayan, A. (2021). KEA3: improved kinase enrichment analysis via data integration. Nucleic Acids Res. *49*, W304–W316. https://doi.org/10.1093/nar/gkab359.

38. Leeming, M.G., O'Callaghan, S., Licata, L., Iannuccelli, M., Lo Surdo, P., Micarelli, E., Ang, C.-S., Nie, S., Varshney, S., Ameen, S., et al. (2021). Phosphomatics: interactive interrogation of substrate–kinase networks in global phosphoproteomics datasets. Bioinformatics *37*, 1635–1636. https://doi.org/10.1093/bioinformatics/btaa916.

39. Patiño-Escobar, B., Talbot, A., and Wiita, A.P. (2023). Overcoming proteasome inhibitor resistance in the immunotherapy era. Trends Pharmacol. Sci. *44*, 507–518. https://doi.org/10.1016/j.tips.2023.05.006.

40. Bhakat, K.K., and Ray, S. (2022). The FAcilitates Chromatin Transcription (FACT) complex: Its roles in DNA repair and implications for cancer therapy. DNA Repair *109*, 103246. https://doi.org/10.1016/j.dnarep.2021.103246.

41. Reijns, M.A.M., Bubeck, D., Gibson, L.C.D., Graham, S.C., Baillie, G.S., Jones, E.Y., and Jackson, A.P. (2011). The structure of the human RNase H2 complex defines key interaction interfaces relevant to enzyme function and human disease. J. Biol. Chem. *286*, 10530–10539. https://doi.org/10.1074/jbc.M110.177394.

42. Jacquemont, C., and Taniguchi, T. (2007). Proteasome Function Is Required for DNA Damage Response and Fanconi Anemia Pathway Activation. Cancer Res. *67*, 7395–7405. https://doi.org/10.1158/0008-5472.Can-07-1015.

43. Neri, P., Ren, L., Gratton, K., Stebner, E., Johnson, J., Klimowicz, A., Duggan, P., Tassone, P., Mansoor, A., Stewart, D.A., et al. (2011). Bortezomib-induced "BRCAness" sensitizes multiple myeloma cells to PARP inhibitors. Blood *118*, 6368–6379. https://doi.org/10.1182/blood-2011-06-363911.

44. Brinkmann, K., Schell, M., Hoppe, T., and Kashkar, H. (2015). Regulation of the DNA damage response by ubiquitin conjugation. Front. Genet. *6*, 98. https://doi.org/10.3389/fgene.2015.00098.

45. Chesi, M., Matthews, G.M., Garbitt, V.M., Palmer, S.E., Shortt, J., Lefebure, M., Stewart, A.K., Johnstone, R.W., and Bergsagel, P.L. (2012). Drug response in a genetically engineered mouse model of multiple myeloma is predictive of clinical efficacy. Blood *120*, 376–385. https://doi.org/10.1182/blood-2012-02-412783.

46. Maura, F., Coffey, D., Braggio, E., Stein, C.K., Sharik, M.E., Du, M.T., Zicchedda, B., Morgan, G.J., Landgren, O., Bergsagel, P.L., and Chesi, M. (2022). Vκ*MYC Mouse Model Recapitulates Key Genomic Defining Events in Multiple Myeloma. Blood *140*, 1540–1541. https://doi.org/10.1182/blood-2022-166614.

47. Tang, S., Ma, D., Cheng, B., Fang, Q., Kuang, X., Yu, K., Wang, W., Hu, B., and Wang, J. (2018). Crucial role of HO-1/IRF4-dependent apoptosis induced by panobinostat and lenalidomide in multiple myeloma. Exp. Cell Res. *363*, 196–207. https://doi.org/10.1016/j.yexcr.2018.01.005.

48. Ray, S., Panova, T., Miller, G., Volkov, A., Porter, A.C.G., Russell, J., Panov, K.I., and Zomerdijk, J.C.B.M. (2013). Topoisomerase IIα promotes activation of RNA polymerase I transcription by facilitating pre-initiation complex formation. Nat. Commun. *4*, 1598. https://doi.org/10.1038/ncomms2599.

49. Xu, H., and Hurley, L.H. (2022). A first-in-class clinical G-quadruplex-targeting drug. The bench-to-bedside translation of the fluoroquinolone QQ58 to CX-5461 (Pidnarulex). Bioorg. Med. Chem. Lett. *77*, 129016. https://doi.org/10.1016/j.bmcl.2022.129016.

50. Mitsiades, N., Mitsiades, C.S., Richardson, P.G., Poulaki, V., Tai, Y.T., Chauhan, D., Fanourakis, G., Gu, X., Bailey, C., Joseph, M., et al. (2003). The proteasome inhibitor PS-341 potentiates sensitivity of multiple myeloma cells to conventional chemotherapeutic agents: therapeutic applications. Blood *101*, 2377–2380. https://doi.org/10.1182/blood-2002-06-1768.

51. Cron, K.R., Zhu, K., Kushwaha, D.S., Hsieh, G., Merzon, D., Rameseder, J., Chen, C.C., D'Andrea, A.D., and Kozono, D. (2013). Proteasome inhibitors block DNA repair and radiosensitize non-small cell lung cancer. PLoS One *8*, e73710. https://doi.org/10.1371/journal.pone.0073710.

52. Bianchi, G., Oliva, L., Cascio, P., Pengo, N., Fontana, F., Cerruti, F., Orsi, A., Pasqualetto, E., Mezghrani, A., Calbi, V., et al. (2009). The proteasome load versus capacity balance determines apoptotic sensitivity of multiple myeloma cells to proteasome inhibition. Blood *113*, 3040–3049. https://doi.org/10.1182/blood-2008-08-172734.

53. Acosta-Alvear, D., Cho, M.Y., Wild, T., Buchholz, T.J., Lerner, A.G., Simakova, O., Hahn, J., Korde, N., Landgren, O., Maric, I., et al. (2015). Paradoxical resistance of multiple myeloma to proteasome inhibitors by decreased levels of 19S proteasomal subunits. Elife *4*, e08153. https://doi.org/10.7554/eLife.08153.

54. Manier, S., Huynh, D., Shen, Y.J., Zhou, J., Yusufzai, T., Salem, K.Z., Ebright, R.Y., Shi, J., Park, J., Glavey, S.V., et al. (2017). Inhibiting the oncogenic translation program is an effective therapeutic strategy in multiple myeloma. Sci. Transl. Med. *9*, eaal2668. https://doi.org/10.1126/scitranslmed.aal2668.

55. Li, S., Fu, J., Lu, C., Mapara, M.Y., Raza, S., Hengst, U., and Lentzsch, S. (2016). Elevated Translation Initiation Factor eIF4E Is an Attractive Therapeutic Target in Multiple Myeloma. Mol. Cancer Ther. *15*, 711–719. https://doi.org/10.1158/1535-7163.Mct-15-0798.

56. Zismanov, V., Attar-Schneider, O., Lishner, M., Heffez Aizenfeld, R., Tartakover Matalon, S., and Drucker, L. (2015). Multiple myeloma proteostasis can be targeted via translation initiation factor eIF4E. Int. J. Oncol. *46*, 860–870. https://doi.org/10.3892/ijo.2014.2774.

57. Walker, Z.J., Idler, B.M., Davis, L.N., Stevens, B.M., VanWyngarden, M.J., Ohlstrom, D., Bearrows, S.C., Hammes, A., Smith, C.A., Jordan, C.T., et al. (2021). Exploiting Protein Translation Dependence in Multiple Myeloma with Omacetaxine-Based Therapy. Clin. Cancer Res. *27*, 819–830. https://doi.org/10.1158/1078-0432.Ccr-20-2246.

58. Kiianitsa, K., and Maizels, N. (2013). A rapid and sensitive assay for DNA-protein covalent complexes in living cells. Nucleic Acids Res. *41*, e104. https://doi.org/10.1093/nar/gkt171.

59. Mees, I., Li, S., Tran, H., Ang, C.S., Williamson, N.A., Hannan, A.J., and Renoir, T. (2022). Phosphoproteomic dysregulation in Huntington's disease mice is rescued by environmental enrichment. Brain Commun. *4*, fcac305. https://doi.org/10.1093/braincomms/fcac305.

60. Cox, J., and Mann, M. (2008). MaxQuant enables high peptide identification rates, individualized p.p.b.-range mass accuracies and proteome-wide protein quantification. Nat. Biotechnol. *26*, 1367–1372. https://doi.org/10.1038/nbt.1511.

61. Szklarczyk, D., Gable, A.L., Lyon, D., Junge, A., Wyder, S., Huerta-Cepas, J., Simonovic, M., Doncheva, N.T., Morris, J.H., Bork, P., et al. (2019). STRING v11: protein-protein association networks with increased coverage, supporting functional discovery in genome-wide experimental datasets. Nucleic Acids Res. *47*, D607–D613. https://doi.org/10.1093/nar/gky1131.